Radial evolution of nonthermal electron populations in the low-latitude solar wind: Helios, Cluster, and Ulysses Observations

Štěpán Štverák,[1,2] Milan Maksimovic,[2] Pavel M. Trávníček,[1,3] Eckart Marsch,[4] Andrew N. Fazakerley,[5] and Earl E. Scime[6]

Received 4 November 2008; revised 6 February 2009; accepted 5 March 2009; published 9 May 2009.

[1] We have performed a statistical study of a substantial amount of solar wind electron velocity distribution functions (eVDFs). In our data set, we combine measurements acquired onboard three spacecrafts (Helios, Cluster II, and Ulysses) in the low ecliptic latitudes covering the heliocentric distance from 0.3 up to 4 AU. In this study, we focus on the nonthermal properties of the measured eVDFs in both the slow and the fast solar wind regimes. The aim of the present study is (1) to provide, for the first time, an analytical model to fit separately all three components of the solar wind eVDFs (i.e., the core, the halo, and the strahl) and (2) to study the fractional densities of the three electron components and also the non-Maxwellian character of the high-energy eVDF tails as a function of the radial distance from the sun. Basically, our study is incremental to the previous studies of the fast solar wind and primarily extends their conclusions on a large number of slow wind observations in the ecliptic plane. We confirm that the halo and the strahl relative densities vary in an opposite way. The relative number of strahl electrons is decreasing with radial distance, whereas the relative number of halo electrons is increasing. The fractional density of the core population remains roughly constant. These findings suggest that there are mechanisms in the solar wind that scatter the strahl electrons into the halo. Also, we find that the relative importance of the nonthermal electrons in the fast solar wind is slightly higher compared to the slow wind.

Citation: Štverák, Š., M. Maksimovic, P. M. Trávníček, E. Marsch, A. N. Fazakerley, and E. E. Scime (2009), Radial evolution of nonthermal electron populations in the low-latitude solar wind: Helios, Cluster, and Ulysses Observations, *J. Geophys. Res.*, *114*, A05104, doi:10.1029/2008JA013883.

1. Introduction

[2] Coulomb collisions are the basic driving mechanism which maintains a plasma locally in the thermodynamic equilibrium. In the solar wind where the plasma is hot and tenuous the effect of Coulomb collisions is limited. Moreover, as the mean free path (m.f.p.) between two collisions rapidly increases with particle velocity (m.f.p. $\propto v^4$), the Coulomb collisions above a certain energy are not effective and the particle velocity distribution functions develop high-energy nonthermal tails. Consequently, significant deviations from an isotropic Maxwellian distribution may occur in the particle velocity phase space. These deviations have indeed been observed by many space instruments in the past for both electrons and protons of the solar wind plasma. The electron velocity distribution functions (eVDFs) observed in the solar wind typically exhibit three different components: a core, a halo and a strahl [*Montgomery et al.*, 1968; *Feldman et al.*, 1975; *Rosenbauer et al.*, 1977; *Pilipp et al.*, 1987a; *Maksimovic et al.*, 2005]. The core electrons are well modeled by a bi-Maxwellian velocity distribution and represent on average about 95% of the total number density. The non-Maxwellian suprathermal tails consist of two separate parts: the halo and the strahl. While the halo is present at all pitch angles, the strahl appears as a beam-like population moving predominantly away from the Sun and is highly focused along the ambient magnetic field. In general, the strahl is observed to be more important in the fast wind than in the slow one [*Rosenbauer et al.*, 1977; *Pilipp et al.*, 1987a].

[3] Study of the radial evolution of these nonthermal eVDF features is important for several reasons. Basically, the bulk of solar wind momentum is carried by protons (because of their large mass with respect to electrons). However, electrons play a major role since they carry the

[1]Department of Space Physics, Institute of Atmospheric Physics, Academy of Sciences of the Czech Republic, Prague, Czech Republic.
[2]LESIA, Observatoire de Paris, CNRS, UPMC, Université Paris Diderot, Meudon, France.
[3]Astronomical Institute, Academy of Sciences of the Czech Republic, Prague, Czech Republic.
[4]Department for Sun and Heliosphere, Max Planck Institute for Solar System Research, Katlenburg-Lindau, Germany.
[5]Mullard Space Science Laboratory, University College London, Dorking, UK.
[6]Department of Physics, West Virginia University, Morgantown, West Virginia, USA.

0148-0227/09/2008JA013883

overall heat flux in the solar wind [*Feldman et al.*, 1975; *Marsch*, 2006]. Furthermore, the precise shape of the eVDFs is fundamental in determining the interplanetary ambipolar electric field which is responsible for the solar wind acceleration in the exospheric theory [*Lemaire and Scherer*, 1971; *Maksimovic et al.*, 1997a, 2001]. Since the core remains almost isotropic or at least symmetric in the plasma rest frame, the heat flux is mostly related to the suprathermal tails of the eVDFs. Furthermore, some authors suggest [e.g., *Scudder and Olbert*, 1979] that because of the weak collisionality, a lasting influence of the boundary conditions in the transition region or even in the corona can be found on the collisionless suprathermals far away from the Sun. The evolution of the eVDF with radial distance can thus contain information about the physical processes in the acceleration region of the solar wind. A detailed description of the nonthermal part of the eVDFs can therefore provide clues to the solar wind initial conditions and acceleration.

[4] From the theoretical point of view, purely collisional fluid models cannot be employed to model the eVDF radial evolution since they do not, by definition, handle the non-Maxwellian suprathermal tails. Conversely, exospheric approaches where collisions are completely neglected [*Lemaire and Scherer*, 1971; *Maksimovic et al.*, 1997a; *Lamy et al.*, 2003; *Zouganelis et al.*, 2004], rely on the eVDF shape in the corona and throughout the heliosphere. In these models the final eVDF shape results from velocity filtration by the interplanetary ambipolar electric field. While the exospheric models can explain the acceleration of the fast solar wind if nonthermal eVDFs are already present in the corona [*Scudder*, 1992; *Maksimovic et al.*, 1997a; *Zouganelis et al.*, 2004], they fail in predicting the precise eVDF shape in the heliosphere. Indeed, in these models there are no electrons above the local escape velocity in the sunward direction and the eVDFs are therefore truncated [*Maksimovic et al.*, 2001]. This is in contradiction with observations even at 0.3 AU. Some improvements to the exospheric approach can be achieved by including the effect of Coulomb collisions. *Lie-Svendsen et al.* [1997] solved the Boltzmann equation with the Fokker-Planck approximation of the collision operator for test particles expanding in a background Maxwellian plasma. Starting their modelization at the base of the corona, these authors produced a skewed eVDF at 0.3 AU qualitatively similar to the observed strahl component. However, the halo component was completely absent in this model. *Pierrard et al.* [1999, 2001] adopted this model with a few modifications. Firstly, they used typical eVDF measured in situ at 1 AU as boundary condition instead of a Maxwellian deep in the corona [*Lie-Svendsen et al.*, 1997] where no detailed observation of eVDFs are available. Secondly, the eVDFs used for the background electrons were more general Lorentzian functions [see *Pierrard and Lemaire*, 1996; *Maksimovic et al.*, 1997b] instead of Maxwellians. Within this scenario, which only included the effect of Coulomb collisions, the authors concluded that (1) nonthermal tails, much less important than at 1 AU, must already be present in the corona in order to explain the observations and (2) that the sunward part of the halo components is present in the inner heliosphere only if it is imposed as a boundary condition at 1 AU.

[5] Collisions are not the only mechanism shaping the observed eVDFs in the solar wind. The departures from a purely Maxwellian distribution naturally produce plasma instabilities and generate waves which in return regulate the initial departures. Wave-particle interactions represent therefore another source of possible electron scattering. As far as the core population is concerned, *Štverák et al.* [2008] presented clear observational evidence that both collision and wave-particle interactions are effective in constraining the temperature anisotropy of the core electron population. While the collisions continuously guide the core properties during the solar wind expansion, the wave-particle interactions come into play only when eVDFs become extremely anisotropic. Similar evidence for wave-particle interactions resulting from plasma instabilities has also been reported for the solar wind protons [*Kasper et al.*, 2003; *Hellinger et al.*, 2006; *Marsch et al.*, 2006]. Concerning the suprathermal component of the solar wind eVDFs, *Gary et al.* [1994] derived from the linear Vlasov theory three kinetic heat flux instabilities which can contribute to the regulation of the solar wind heat flux, i.e., the regulation of the halo and strahl components: Alfvén, magnetosonic and whistler instabilities. The effect of whistler waves was further numerically examined by *Vocks et al.* [2005], *Gary and Saito* [2007] and *Saito and Gary* [2007] with particle-in-cell simulations. These authors showed theoretically that whistler waves are capable of forming both the halo and strahl components and are effective in scattering of strahl electrons into the halo.

[6] However, and contrary to the core component, clear observational evidence demonstrating the role of waves in shaping the nonthermal halo and strahl components has still not been reported.

[7] From the observational point of view, the nonthermal part of the solar wind eVDFs was originally studied in detail by *Feldman et al.* [1975] and later by *Pilipp et al.* [1987a, 1987b]. The halo and strahl were modeled altogether as a drifting bi-Maxwellian with respect to the solar wind plasma frame. It was shown that the difference between the core and the halo charge fluxes (due to the relative core-halo drift) are in a good agreement with the zero-current relation as it is necessary to provide a zero current in the solar wind. Also, the nonthermal electrons were shown to be the main source of the total electron heat flux. The natural choice of a Maxwellian distribution allows an easier comparison with theoretical results. The Maxwellian VDF corresponds to a medium in local thermodynamic equilibrium which is the classical assumption in theoretical approaches, namely the MHD fluid descriptions. However, even a sum of two Maxwellians does not perfectly reflect the overall shape of observed eVDFs. As an alternative to the classical sum of two bi-Maxwellians, one for the core and one for the halo plus the strahl, *Maksimovic et al.* [1997b] used a single Lorentzian Kappa function to fit the entire eVDFs. At low speeds the Kappa distribution is nearly Maxwellian. It decreases as a power law at speeds greater than the thermal speed. The Kappa function can thus handle to a certain degree both the thermal core and the nonthermal tails. More recently, *Maksimovic et al.* [2005] examined the relative importance of the nonthermal electrons in the fast solar wind as a function of the increasing radial distance from the Sun. These authors proposed that the best analytical model

Table 1. Measurements of eVDFs Used in This Study Include Data From Several Spacecraft: Helios 1 and 2, Cluster II, and Ulysses[a]

S/C	Instrument	Period	Distance (AU)	Samples
HELIOS	I2	1975–1978	0.3–1.0	≈200,000
CLUSTER II	PEACE	2002–2003	1.0	≈25,000
ULYSSES	SWOOPS	1990–1991	1.2–3.95	≈15,000

[a]The data set includes roughly 240,000 samples covering the radial distances from the sun from 0.3 to 4 AU.

for the core and halo is constituted by the sum of a bi-Maxwellian for the core and a bi-Kappa function for the halo. Concerning the strahl, they did not propose any analytical model but rather computed its characteristics numerically by subtracting the core-halo model from measured eVDFs. The main result obtained by *Maksimovic et al.* [2005] for the fast wind is that the strahl relative density is declining with increasing radial distance, whereas the halo importance increases. These findings, together with those of *McComas et al.* [1992], who showed that the core relative density remains almost unaffected during the expansion and those of *Hammond et al.* [1996], who showed that the strahl angular width broadens with increasing radial distance, support the scenario of strahl electrons being scattered into the halo, probably by waves processes.

[8] The aim of the present study is (1) to provide for the first time an analytical model to fit separately all three components of the solar wind eVDFs (i.e., the core, halo and strahl); and (2) to extend the study of *Maksimovic et al.* [2005] to the slow solar wind observed in the ecliptic plane. Compared to *Maksimovic et al.* [2005], we use a slightly different analysis technique. We modified the two-component analytical model, i.e., the sum of one bi-Maxwellian and one bi-Kappa function for the core and the halo respectively, and improved it to fit also, for the first time analytically, the strahl component of the observed eVDFs. In comparison to *Maksimovic et al.* [2005] our statistical study is based on a much larger data set which includes data acquired on the Helios 1 and 2, Cluster II and Ulysses spacecraft over the radial range from 0.3 AU up to almost 4 AU. In section 2, we describe our data set more in detail and introduce the data processing techniques. Our results on the strahl analytical modeling and radial evolution of the eVDFs suprathermal components are then presented and discussed in section 3. Finally, a summary and conclusions are given in section 4.

2. Data Set and Data Analysis Techniques

[9] For the statistical study of solar wind properties, we have gathered a large number of measured eVDFs combining observations from three different spacecraft. A detail description of the full data set and of the associated space instruments is given in section 2.1. The fitting procedures which we use for the analysis of the measured eVDFs are then explained in the following section 2.2.

2.1. Data

[10] In order to cover a sufficiently large range of radial distances together with a sufficiently large range of solar wind bulk speed conditions, we combine electron measurements obtained by the Helios 1 and 2, the Cluster and the Ulysses spacecraft. All measured data were acquired in the low ecliptic latitudes and cover altogether radial distances from 0.3 up to almost 4 AU. The data set thus represents the largest possible range of heliocentric distances in the ecliptic. However, since each one of the three spacecraft operated in a different time period, the data set combines several solar cycles and different periods of the solar activity. The overall description of our data set is given in Table 1. For our analysis we split all samples in two groups: the slow and the fast solar wind. We denote as the slow and fast regimes of the solar wind all samples with an proton bulk speed lower than 500 km/s and larger than 600 km/s respectively.

[11] Onboard the two Helios spacecraft electrons were measured with almost identical electron analyzers [*Schwenn et al.*, 1975; *Rosenbauer et al.*, 1977]. The probes continuously spun around an axis oriented perpendicular to the ecliptic plane. By use of the spacecraft rotation, the electron analyzer placed in the equatorial plane of the spacecraft recorded two-dimensional electron distribution functions. These velocity distributions cover an energy range between 0.5 and 1658 eV in 32 energy channels and 8 angular bins uniformly distributed in the polar plane. The radial coverage of both Helios probes ranges from 0.3 to 1 AU. For our analysis we use only those measurements for which the magnetic field vector is close enough to the ecliptic plane, that is when $B_z/|B| < 0.1$ [see *Štverák et al.*, 2008, for more details]. We also require the magnetic field vector to be very close, with a maximum deviation of 10°, to the axis of one of the angular bins. These conditions guarantee to have a good estimate of the eVDF in the ($v_\perp$, $v_\parallel$) plane, where the directions $\perp$ and $\parallel$ are with respect to the local magnetic field vector.

[12] The four satellites of the Cluster II mission [*Escoubet et al.*, 1997] measure electrons thanks to the PEACE instruments which are identical on each spacecraft [see *Johnstone et al.*, 1997, for a detail description]. The full energy range of all PEACE instruments scales from 0.6 eV to 26.5 keV. For our data set we use the SPINPAD data product which provides two-dimensional eVDFs covering one half of the ($v_\perp$, $v_\parallel$) plane in 13 angular bins. In this study we use only data from Cluster 3. Since the spacecraft spends a part of its orbit in the Earth's magnetosphere we selected only periods when the satellite was in the unperturbed solar wind, not magnetically connected to the Earth's bow shock.

[13] The data set is completed with measurements from the Ulysses spacecraft covering a radial range from 1.2 to 4 AU. Onboard Ulysses the eVDFs were measured by the SWOOPS instrument [*Bame et al.*, 1992]. Its construction enables both two-dimensional and also full (95% of the unit sphere) three-dimensional electron measurements covering an energy range from 1.6 to 862 eV. We take data acquired only during the first part of the mission when the spacecraft traveled in the ecliptic plane toward Jupiter. The out of ecliptic fast solar wind measurements have already been analyzed by *Maksimovic et al.* [2005]. The three-dimensional eVDFs are projected in the ($v_\perp$, $v_\parallel$) plane and then analyzed in the same way as it is done for eVDFs from Helios and Cluster.

[14] In order to get proper estimation of the electron properties from the measurements, several corrections on

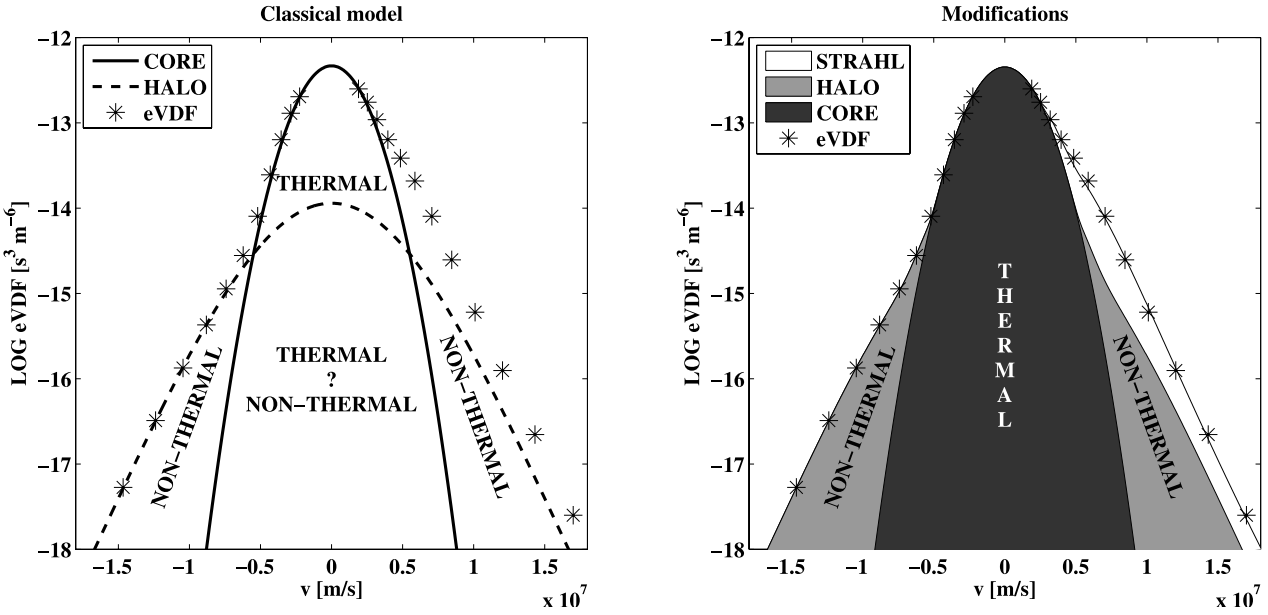

Figure 1. (left) Classical models for the halo component include both electrons in the thermal equilibrium being the part of the core and nonthermal electrons at higher energies wherein tails are dominant above the Maxwellian core. (right) The model used for this study separates the whole eVDF into the thermal (core) and nonthermal part (halo and strahl), giving a better estimation of their relative densities.

the eVDFs have to be made. Typically the measured eVDFs are influenced by the positive S/C potential accelerating electrons to higher energies. The measured energy bins have thus to be corrected [see *Song et al.*, 1997; *Salem et al.*, 2001, for instance]. In addition, the low energy bins are polluted by the cold photoelectrons emitted from the spacecraft itself. The influence of photoelectrons can be removed by introducing a given threshold energy and cutting off the whole part of the eVDF below this chosen energy limit. Commonly the final step is to apply a transformation from the S/C reference frame into the solar wind plasma frame. The S/C velocity being negligible, this step consists in subtracting the solar wind bulk speed, taken from ion measurements in our case, from the measured electron velocities.

[15] The S/C potential was not measured onboard Helios. We therefore estimate this potential by calibrating the measured eVDF to the total ion density. In the case of Cluster, the S/C potential is available from *in situ* measurements [*Gustafsson et al.*, 1997]. The Ulysses data samples were already corrected with a more sophisticated procedure. A complete description of this method is given by *Scime et al.* [1994b]. In brief, all the electron trajectories were mapped using the planar sheath approximation of the S/C electric field. This technique thus corrects not only the initial energy of the impacting electrons but also their actual velocity direction before entering the S/C sheath.

2.2. Fitting Procedures

[16] As we already mentioned in the introduction, the solar wind eVDFs are composed by a sum of several components: a thermal core, which typically represents more than 95% of the total electron number density, a hotter suprathermal halo, representing the nonthermal tails which are present at all pitch angles, and a highly magnetic field–aligned strahl.

[17] The most recent fitting procedure proposed to model most precisely the solar wind eVDFs [*Maksimovic et al.*, 2005] can be summarized as follows. As a first step, the part of the eVDFs, from which the strahl is absent, is fitted with the sum of one bi-Maxwellian (f_c) and one bi-Kappa function (f_h) for the core and halo respectively. f_c and f_h are defined over the whole velocity phase space $v_\perp$, $v_\parallel$, where the subscripts $\parallel$ and $\perp$ are with respect to the local magnetic field direction. Once f_c and f_h are determined, they are removed from the observed eVDF (f_{obs}) and the strahl characteristics such as the density are obtained by integrating $f_{obs} - f_c - f_h$ over the velocity phase space. Even though it represents an improvement to the previous models (a sum of two bi-Maxwellians or one single bi-Kappa function), this fitting procedure is still not fully satisfactory for two reasons. Firstly an analytical description for the strahl component is still necessary for estimating more accurately some fundamental parameters such as the electron heat flux. In this study we propose an analytical form for the strahl. Secondly, there is a clear ambiguity when computing separately the core and halo number densities in order, for instance, to study the radial evolution of their respective fractions of the total number density. This ambiguity is sketched in Figure 1. On the left hand side of Figure 1, it is not possible to decide whether an electron in the thermal velocity/energy range belongs to the core population or to the halo one. Therefore based on the measured eVDFs, it is not possible to uniquely define the model function of the halo component in the thermal energy range. Also, since the electrons in the thermal energy range represent a large fraction of the total halo density when f_h is defined over the

whole velocity phase space, the resulting density of the halo component in the model from the work of *Maksimovic et al.* [2005] does not reflect the pure density of the suprathermal tails of the observed eVDFs. In the present study, we want to characterize the true difference between the theoretical Maxwellian distribution predicted for a gas in a local thermal equilibrium and eVDFs observed in the solar wind more precisely. We solve the described ambiguity between the core and halo electrons by restricting f_c and f_h to respectively the thermal and suprathermal parts of the velocity phase space. This is illustrated on the right-hand side of Figure 1. By doing so we can study separately the properties of the thermal electrons which are more bounded by collisions and the suprathermal ones which are almost collisionless.

[18] The model proposed for this study is composed of a sum of three analytical forms for each of the basic eVDF components observed in the solar wind, namely the core (f_c), halo (f_h) and strahl (f_s)

$$f = f_c + f_h + f_s. \tag{1}$$

[19] For the core component we use a classical bi-Maxwellian function drifting in the parallel direction with respect to the magnetic field. Thus f_c reads as

$$f_c = A_c \exp\left[-\frac{m}{2k}\left(\frac{1}{T_{c\perp}}v_\perp^2 + \frac{1}{T_{c||}}\left(v_{||} - \Delta_c\right)^2\right)\right], \tag{2}$$

where m is the electron mass, k is the Boltzmann constant, $T_{c\perp}$ and $T_{c||}$ are the core perpendicular and parallel temperatures respectively and Δ_c is the drift velocity in the proton bulk speed frame. The normalization factor A_c is equal to

$$A_c = n_c\left(\frac{m}{2\pi k}\right)^{3/2}\frac{1}{T_{c\perp}\sqrt{T_{c||}}}, \tag{3}$$

where n_c is the core number density.

[20] For the halo population, we still use a bi-Kappa function as in the work of *Maksimovic et al.* [2005] but we introduce one major modification in order to reach our requirements, that is the clear separation of the nonthermal electrons from the thermal ones. We require the inner part of the bi-Kappa function hidden in the thermal core to be truncated by the use of a flat top like function ($f_{h,ft}$). The analytical form for the halo (f_h) is then

$$f_h = \left(1 - f_{h,ft}\right)\cdot f_{h,\kappa}. \tag{4}$$

[21] In equation (4), $f_{h,\kappa}$ is the classical bi-Kappa function defined as

$$f_{h,\kappa} = A_h\left(1 + \frac{m}{k(2\kappa_h - 3)}\left(\frac{v_\perp^2}{T_{h\perp}} + \frac{v_{||}^2}{T_{h||}}\right)\right)^{-\kappa_h - 1}, \tag{5}$$

where m, k, $T_{h\perp}$ and $T_{h||}$ have the analogous meaning as in equation (2) and the κ_h parameter determines the power law decrease of the suprathermal tails. The bi-Kappa function is normalized by

$$A_h = n_{h\kappa}\left(\frac{m}{\pi k(2\kappa_h - 3)}\right)^{3/2}\frac{1}{T_{h\perp}\sqrt{T_{h||}}}\frac{\Gamma(\kappa_h + 1)}{\Gamma(\kappa_h - 1/2)}, \tag{6}$$

where $n_{h\kappa}$ is the zero-order moment of the Kappa function and $\Gamma()$ is the Gamma function. Because of the truncation, $n_{h\kappa}$, however, does not expresses the number density of the halo.

[22] In equation (4), $f_{h,ft}$ is the so-called "flat top" function defined in our case as

$$f_{h,ft} = \left[1 + \left(\frac{m}{2k\delta}\left(\frac{v_\perp^2}{T_{c\perp}} + \frac{\left(v_{||} - \Delta_c\right)^2}{T_{c||}}\right)\right)^p\right]^{-q}. \tag{7}$$

This function is defined in such way that it creates a plateau (at level of one) symmetric with respect to the origin. At the edge of this plateau $f_{h,ft}$ rapidly falls with increasing velocity to zero. The width of the flat top is controlled via the parameter δ. The parameters p and q, which determine the shape of the edge of the plateau, are constant in this model and are equal to 10 and 1 respectively. These values are empirically found to be convenient for our analysis. Note that due to the truncation, the correct density of the halo component has to be computed by integrating equation (4) over the whole velocity phase space. Also, the parameters $T_{h\perp}$ and $T_{h||}$ similarly do not correspond to the halo temperatures as it is the case for the core component.

[23] Finally for the strahl population we also use a bi-Kappa function modified in such a way that it models only those high-energy electrons of the measured eVDF that are streaming away from the Sun and are aligned along the local magnetic field line. Note that some special configurations when the direction of the magnetic field is locally inverted [see, e.g., *Crooker et al.*, 2004] may change the strahl propagation. Such observations of sunward moving or even bidirectional strahl electrons have been reported [see *Gosling et al.*, 1987, 1993, for instance]. In general, the strahl exhibits properties similar to a beam-like population overrunning the core and halo electrons. Therefore we use an analytical model with a positive drift in the parallel direction with respect to the plasma frame. More precisely, in the antisunward direction we use a classical bi-Kappa function with a parallel temperature corresponding to the measured data. In the sunward direction the model is truncated by decreasing the parallel temperature with a given factor. This truncation excludes therefore the thermal core electrons from the strahl population. The analytical formula for the strahl is then

$$f_s = A_s\left(1 + \frac{m}{k(2\kappa_s - 3)}\left(\frac{v_\perp^2}{T_{s\perp}} + D\frac{\left(v_{||} - \Delta_s\right)^2}{T_{s||}}\right)\right)^{-\kappa_s - 1} \tag{8}$$

with

$$\begin{array}{ll} D = 1 & for \quad v_{||} \geq \Delta_s \\ D = \Theta & for \quad v_{||} < \Delta_s \end{array} \tag{9}$$

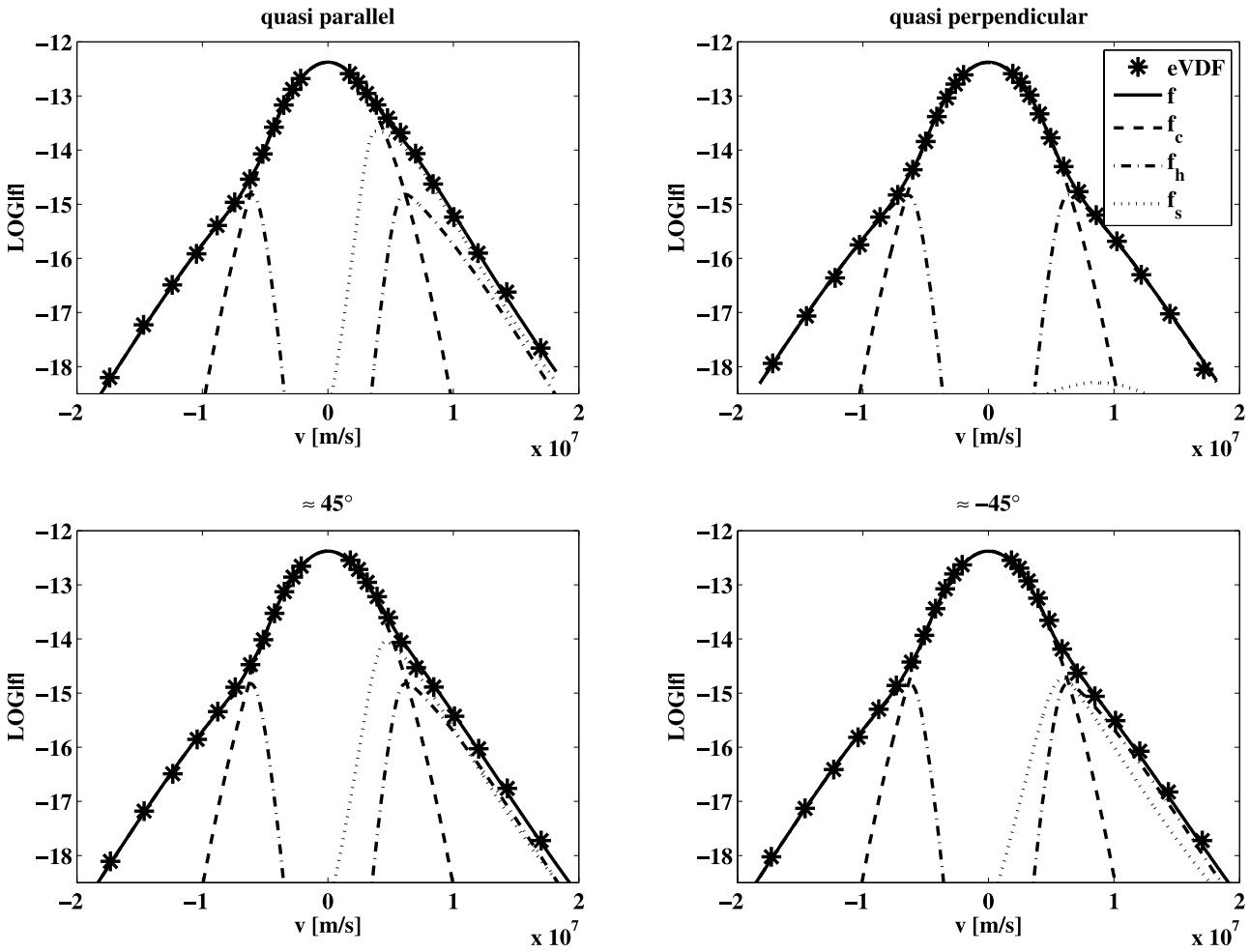

Figure 2. Sample fit of a measurement from Helios using the analytical model proposed for our study. All three components of the measured eVDFs are included, and both halo and strahl are truncated in the thermal part of the distribution. The asterisks, dashed line, dash-dotted line, and dotted line represent the measured eVDF, core, halo, and strahl population, respectively. In these four panels, all cuts through the eight azimuthal bins measured onboard Helios are displayed. The strahl is strongest in the antisunward parallel direction, while it is almost negligible in the perpendicular one. The halo is presented at all pitch angles.

where m, k, $T_{s\perp}$, $T_{s\|}$ and κ_s have analogous meaning as in equation (5), Θ in the case of $v_\| < \Delta_s$ causes the eVDF to be truncated in the sunward direction and Δ_s is the drift of the beam with respect to the proton plasma frame. The function is normalized by

$$A_s = n_s \frac{2\sqrt{\Theta}}{\sqrt{\Theta+1}} \left(\frac{m}{\pi k(2\kappa_s-3)}\right)^{\frac{3}{2}} \frac{1}{T_{s\perp}\sqrt{T_{s\|}}} \frac{\Gamma(\kappa_s+1)}{\Gamma(\kappa_s-1/2)}, \quad (10)$$

so that n_s gives directly the strahl number density. During the fitting we do not adjust the parameter Θ. Actually the value of Θ is fixed to 10, this ensures a sufficient cutoff inside the thermal core velocity range. For our needs this value was empirically found to be convenient over the whole range of the observed eVDF characteristics.

[24] Altogether, we have fourteen free parameters when adjusting equation (1), i.e., n_c, $T_{c\perp}$, $T_{c\|}$, Δ_c, n_h, $T_{h\perp}$, $T_{h\|}$, κ_h, δ, n_s, $T_{s\perp}$, $T_{s\|}$, κ_s and Δ_s. Instead of fitting directly the measured values (f_m), we fit the logarithm ($\log f_m$). This is done in order to take into account the high-energy part of the eVDFs, which is some orders of magnitude smaller than the central thermal part of the distributions. Since our model eVDF depends nonlinearly on the fitted parameters, we use an iterative fitting technique based on the well known Levenberg-Marquardt algorithm [*Marquardt*, 1963] to minimize the χ^2 function. The fitting procedure consists of several steps. First the initial guesses of the parameters for the core, halo and strahl are performed separately and then a final fine adjusting fitting with all parameters together is accomplished. Two of the model components, the core and the strahl, can drift with respect to the plasma frame. Therefore we also check the zero-current condition as it was done for instance by *Feldman et al.* [1975] (see Appendix B). An example of an outcome of our fitting procedure is shown on Figure 2 for a sample of Helios data. In these four panels, all of the eight azimuthal bins measured onboard Helios are displayed with asterisks and the model eVDF and its three components, the core, the

halo and the strahl, are represented with the solid, dashed, dash-dotted and dotted line respectively. The two main features of our new model are visible. The model functions for the high-energy tails are truncated on the thermal core velocity range, and the fit describes very well the complete eVDF including the asymmetric part in the parallel direction, i.e., the strahl. We chose a Helios data sample for the demonstration of the new model because of its relative simplicity. For Cluster and Ulysses observations the quality of our fitting procedure is similar.

3. Results of a Statistical Analysis in Low-Latitude Solar Wind

[25] We have gathered more than 240,000 various solar wind eVDFs acquired in the low ecliptic latitudes. However, not all of the available samples were fitted by the model (1). In order to exclude measurements inappropriate for our analysis we imposed on our data set several restrictions.

[26] For the Helios data, we analyze only measurements where the angle between the magnetic field vector and the axis of some of the eight azimuthal bins is sufficiently small. We impose an upper limit value of 10°. Less than 40% of Helios data set obeys this strong restriction. This approach however guarantees that at least one of the measured angular bins gives a good description of the strahl component. We apply a similar condition also to the Ulysses data: only measurements with enough data points in the strahl direction are taken for further analysis. For the Cluster data the first and last angular bins of the SPINPAD data product are always parallel to the local magnetic field line. Therefore no restriction with respect to strahl characteristics are needed.

[27] Next, the S/C potential was not measured directly onboard Helios, therefore we first estimated its value for our further analysis. Consequently, we restricted the Helios data to samples with S/C potential estimated to be positive. Finally, roughly only 50,000 samples from our initial data set satisfied all these restrictions and were processed by our fitting procedure.

[28] We evaluate also the goodness of the fit, in order to better compare samples from different instruments. We compute a standard error–like parameter ϵ defined by $\epsilon = (\chi^2/(N-1))^{1/2}$, where χ^2 is the sum of the squared deviations of the fit and N is the number of fitted points for the corresponding data sample. For further analysis, we keep only fits where this standard error satisfies $\epsilon \leq [\mu(\epsilon) + 2/3\ std(\epsilon)]$, here $\mu(\epsilon)$ is the mean value of ϵ over all eVDF samples and $std(\epsilon)$ is the standard sample deviation of the mean value. Furthermore, some of the samples are removed from the analysis by reason of unrealistic resulting parameters. For these samples, the standard error ϵ fulfills our condition for the quality of the fit but the resulting characteristics of the measured eVDF are considerably different from those typically observed, and the estimated moments do not correspond to expected conditions in the solar wind (e.g., core temperatures larger than 10^6 K which is comparable to the temperature in the solar corona). Finally, only those results satisfying all these conditions imposed on the quality of the fit and on the resulting moments, about 70% of all fitted samples, are used for our final statistics.

[29] By use of data from three different spacecraft we cover a heliocentric distance from 0.3 AU up to almost 4 AU. In this range we examine the radial profiles of the main characteristics of all three eVDF components. We look mainly at the evolution of the relative densities of the three eVDF components. We have to remind here that while the core and strahl densities are expressed directly by n_c in equation (2) and n_s in equation (8) respectively, the halo density n_h has to be computed numerically by integrating equation (4) over the whole velocity phase space as

$$n_h = \iiint_{\mathcal{R}^3} f_h d\mathbf{v}. \tag{11}$$

Furthermore, by computing averages from all parameters, we provide an overview of the variation of the model eVDF shape with increasing radial distance.

[30] Typically, three major regimes of solar wind flows are observed by the space missions [*Marsch*, 2006]. The first one is the steady fast wind originating from the open magnetic field lines in the coronal holes. The second is the unsteady slow wind coming from edges of temporarily open streamers or from opening loops and active solar regions. And finally, as a last solar wind regime we consider transient flows that are dominated by the so-called coronal mass ejections (CMEs) prevailing during solar maximum cycle. In our study we focus on the main two regimes, i.e., the slow and fast solar wind. These two regimes are examined separately in the following two subsection. We omit the transient disturbances for several reasons. The transient regime of the solar wind is associated with episodic solar events like ejections of material into interplanetary space from coronal regions. Therefore for a large data set covering a sufficiently long time interval, the effect of such events on the overall average characteristics of the solar wind is assumed not to be significant. As a byproduct of our analysis, we study the breakpoint energy of the electron population, i.e., the energy at which the eVDF loose its thermal (Maxwellian) properties and starts to develop the nonthermal tails. We examine also the satisfaction of the zero-current condition in the solar wind. These results are discussed in the Appendices A and B respectively.

3.1. eVDF Radial Evolution in Slow Wind

[31] We classify as a slow wind all the samples with a proton bulk speed lower than 500 km/s. This represents more than 90% of our whole data set. The density profiles for all three eVDF components and for the sum of the nonthermal parts (i.e., the halo and the strahl) are shown on Figure 3. The whole data set is divided into radial bins in which the mean values of the respective densities are computed. The mean values are represented by squares for the core, diamonds for the halo, circles for the strahl and stars for the sum of the halo and the strahl. Error bars are of the order of the symbols size in this case.

[32] For an isotropic steady state expansion the solar wind density should decrease as r^{-2}. In the solar wind, this should be the case of the core component. In Figure 3 we plot this theoretical profile (dots) for reference. It can be seen that this profile is in a good agreement with the radial evolution of the core density as expected. We find that this

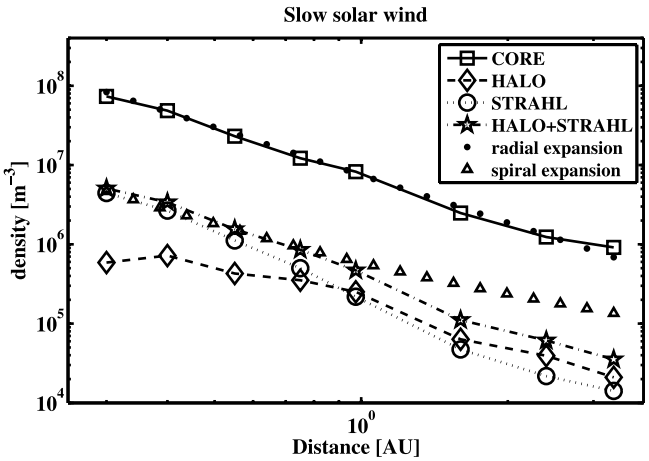

Figure 3. Radial evolution of the density profiles in the slow solar wind. Symbols represent mean values as computed from the fitting results in several radial bins. The error bars are of the order of the symbol size. Two theoretical reference profiles for a pure radial expansion and an expansion following the spiral magnetic field are plotted with dots and triangles, respectively. The solid line with squares, dashed line with diamonds, dotted line with circles, and dash-dotted line with stars represent the radial evolution of the core, halo, strahl, and sum of the strahl and halo, respectively.

latter varies as $r^{-2.03\pm0.08}$, which indicates that the mean core density follows well, within the uncertainties, a steady state radial outflow. The halo and strahl profiles show different trends. While the strahl slope is slightly steeper, the halo density profile is flatter up to 1 AU. This difference demonstrates that the evolution of the nonthermal electron densities is more complex than a pure radial expansion.

[33] For the strahl component we cannot use the simplified approach of an isotropic expansion. Contrary to the core, the strahl is rather expanding along the magnetic field which can be approximated as radial only up to a limited distance. In *Scime et al.* [1994a] the authors have shown that a quantity expanding along the magnetic field in a spiral configuration [*Parker*, 1963] is rather proportional to

$$\propto \frac{1}{r^2}\sqrt{1+\left(\frac{r\omega}{v_{sw}}\right)^2}, \qquad (12)$$

where r is the heliocentric distance, ω is the angular speed of the Sun's rotation and v_{sw} is the solar wind speed. For a sufficiently small distance, equation (12) can still be replaced by $\sim r^{-2}$ but with increasing r this formula tends more to $\sim r^{-1}$. The theoretical profile equation (12) for a slow solar wind with v_{sw} = 400 km/s is plotted in Figure 3 with triangles. However, obviously neither this theoretical approach is matching with our observations. It is important to note that even by adjusting v_{sw} in equation (12) we cannot achieve the observed characteristics. Therefore other processes must explain the radial scaling of the density of the nonthermal eVDF components.

[34] In addition to the radial profiles of the densities themselves, it is very useful to compute the radial variations of the relative number densities, i.e., the ratio of the density of individual eVDF components to the total electron density. On Figure 4 we plot these relative densities $n_{*,rel} = n_*/n_e$ of the eVDF components with respect to the total one n_e, that is the sum of the core, halo and strahl ($n_e = n_c + n_h + n_s$), again as a function of the heliocentric distance. The relative density of the core, halo, strahl and the sum of the halo and strahl are represented by solid line with squares, dashed line with diamonds, dotted line with circles and dash-dotted line with stars respectively. The vertical lines represent the error bars of the corresponding mean values in every radial bin. The most interesting result shown on Figure 4 is the clear opposite trend between the halo and strahl relative densities. While the fractional number density of the strahl decreases with the radial distance, starting approximately at 6% at 0.3 AU and being less than 2% beyond 3 AU, the halo relative density increases from less than 1% at 0.3 AU to more than 3% at the end of the observed radial range. There is another important result on Figure 4: by extrapolating the relative density of the halo component below 0.3 AU closer to the Sun, the contribution of halo electrons seems to be almost negligible with respect to the total electron density. The relative density of the summed nonthermal parts remains however more or less constant during the solar wind expansion as it is the case of the relative density of the thermal core. From our fitting it appears that the nonthermal electrons represent roughly 5–7% of the total electron number density, this fraction being constant with distance. These findings are similar to those observed by *Maksimovic et al.* [2005] in the fast wind except for the nominal values of the relative densities, which is due to the use of different fitting procedures. Our observations therefore support theories [*Gary et al.*, 1994; *Vocks et al.*, 2005; *Gary and Saito*, 2007; *Saito and Gary*, 2007]

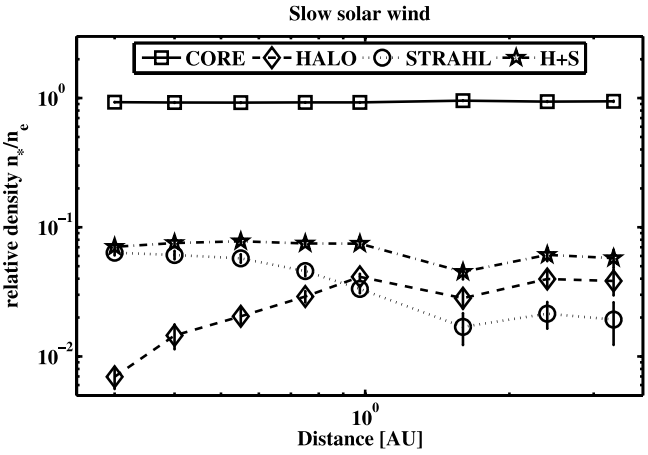

Figure 4. Radial evolution of the relative densities of the eVDF components for the slow solar wind observations. Symbols represent mean values with their error bars. The solid line with squares, dashed line with diamonds, dotted line with circles, and dash-dotted line with stars represent the core, halo, strahl, and sum of strahl and halo, respectively. The total number of nonthermal electrons remains almost constant along the observed range. The strahl density decreases, while the halo one concurrently grows, indicating electrons scattering between these two components.

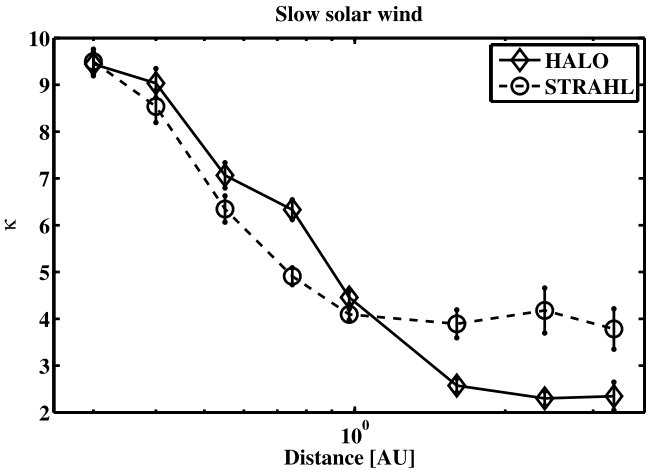

Figure 5. κ parameter can serve as a measure of the nonthermal state of an electron population. Here, we plot the mean κ parameter of the halo (dashed line with diamonds) and strahl component (dotted line with circles) in the slow solar wind as a function of the radial distance. Both of them are decreasing, indicating stronger eVDF tails at larger distances from the sun.

proposing mechanisms which can be responsible for the scattering of the strahl electrons into the halo while keeping the thermal core unaffected.

[35] Actually, the scattering of the strahl electrons can also partly explain the disagreement between the theoretical profile equation (12) and the observed one plotted in Figure 3. While in equation (12) we suppose the rarefaction of the strahl due to the expansion only, on Figure 4 we show that the decrease of the strahl density is also caused by the transfer of strahl electrons into other eVDF components.

[36] Another information about the nonthermal state of the observed eVDFs can be obtained from the parameter κ for both the halo and strahl components. The κ distribution is defined such as that with increasing κ, the function is becoming more and more Maxwellian (actually the distribution is almost Maxwellian for $\kappa \geq 10$). Therefore we can use κ as a measure of the nonthermal character of the eVDF tails. The larger is κ the less pronounced are the tails. The radial evolution of κ is displayed on Figure 5. Here the dashed line with diamonds and dotted line with circles represent the κ parameter of the halo and strahl components respectively. For both of them, κ is decreasing with increasing radial distance. This means that as the solar wind expands, both the halo and the strahl become more and more non-Maxwellian.

[37] In Figure 6, we summarize the radial evolution of the observed eVDFs in the slow solar wind. We display the radial evolution of the model distribution function (1) computed using the average parameters from the fitting process. Four different radial distances are compared: 0.35 AU (dotted line), 0.55 AU (dashed line), 0.75 AU (dash-dotted line) and 2.5 AU (solid line). Figure 6 thus gives very nice picture of the radial evolution of a typical eVDF shape in the slow solar wind. For every radial bin, we plot the cut of the model eVDF along the velocity parallel to the magnetic field. In the top left panel we plot the model eVDF as it results from the fitting procedure. One can see the natural cooling and rarefaction caused by the solar wind expansion. In order to better compare the radial evolution of the shape of the eVDF, we plot the normalized model functions in the remaining three panels. The normalization is done in such a way that the maximum of f is set to 1 and the velocity is given in $v_{\mathrm{th,c}}$ units, where $v_{\mathrm{th,c}} = \sqrt{2kT_{c||}/m}$ is the parallel thermal speed of core electrons. Such normalizations remove the radial trends (the cooling and rarefaction) of the core component caused by the solar wind expansion. The core component is represented in these three panels with dots. The top right panel represents the whole model eVDF while the bottom panels show the halo and strahl components respectively. All the properties discussed on Figures 3, 4 and 5 are also visible on Figure 6. The halo tails density is increasing at the expense of the strahl (as on Figure 4). The nonthermal character of both the halo and the strahl increases with the heliocentric distance (as on Figure 5). The bottom right panel of Figure 6 is very interesting. It allows to better visualize the strahl scattering. From Figure 6 it appears that strahl electrons around the core boundary, where the core electrons are still enough numerous, thus close to the thermal regime, decreases significantly during the expansion and probably scattered in other pitch angles into the halo population. This behavior can mean that Coulomb collisions could also act as one of the strahl scattering mechanisms.

3.2. eVDF Radial Evolution in Fast Wind

[38] The fast solar wind is in general considered as a steady state outflow compared to the less stationary slow wind regime. It is typically less dense than the slow wind and the eVDF nonthermal features are thus observed to be more important. For our statistics we have selected only eVDF samples with measured proton bulk speed greater than 600 km/s. In our data set which includes inecliptic observations, only roughly 10% of the total number of eVDF samples represent the fast solar wind regime. Moreover, there are only about one hundred samples with the given bulk speed condition in the Ulysses radial range (1.2–4 AU). This can yield therefore larger uncertainties in the estimation of the mean eVDF properties. Nevertheless, in order to make the study complete, we present here the results concerning the fast solar wind, even though the statistical conclusions, in this case, will have to be taken with caution.

[39] All figures concerning the fast wind are analogous to the previous section 3.1 describing the slow wind. The radial evolution of the electron number densities is shown on Figure 7. As for the slow wind, we plot all three eVDF components plus the sum of the two nonthermal parts. Again, the core density decreases as $\sim r^{-2}$. The exact law for the core density in the fast wind is proportional to $\propto r^{-2.11\pm0.17}$, with the exponent slightly smaller compared to *Maksimovic et al.* [2005]. The radial trends of the halo and strahl densities are also similar to the slow wind case. At 0.3 AU the strahl density is higher than the density of the halo but it falls faster with radial distance. Therefore the halo density overcomes at certain distance, around 1 AU, the strahl one. The radial profile of the strahl density decreases still slightly more steeply than the prediction for an expansion along the spiral oriented magnetic field. The

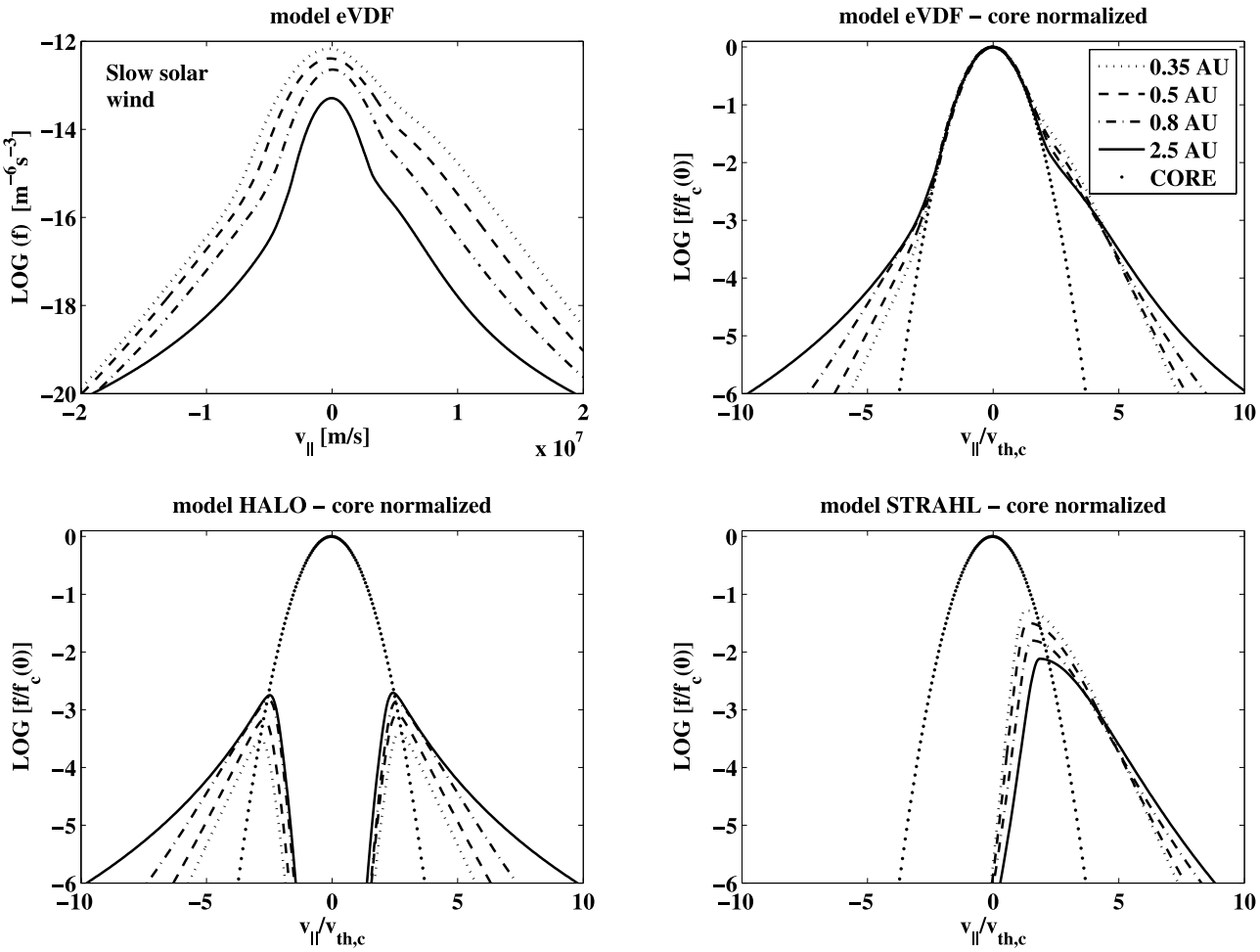

Figure 6. Radial evolution of a model eVDF function in the slow solar wind. Model functions are plotted using average values of all parameters as resulting from the fitting at four different radial distances: 0.35 AU (dotted line), 0.55 AU (dashed line), 0.75 AU (dash-dotted line), and 2.5 AU (solid line). Except for the top left panel, the model eVDF functions are normalized so that the value at the peak equals to 1 and the velocity is scaled by $v_{th,c}$ in order to remove the core radial trends. In the bottom panels, the halo and strahl component evolution is compared with the normalized core. With increasing radial distance, the strahl electrons close to the thermal core are scattered, and at the same time, the halo develops stronger tails and its relative importance is growing.

theoretical profile for a spiral expansion equation (12), plotted with triangles on Figure 7, is now computed for the solar wind speed v_{sw} = 650 km/s.

[40] The relative densities of the eVDF components are displayed on Figure 8. Globally as for the slow wind case, the results for the fast wind tend to support the theory of strahl electrons being scattered into the halo, however, with two noticeable differences. First the sum of the halo and strahl relative densities is more variable with radial distance compared to the almost constant trend observed in the slow wind case. This could be due to either a statistical effect caused by a lack of fast wind samples, or to some possible interplay between the core and strahl/halo electrons as well. Secondly, as already reported by several previous studies [*Feldman et al.*, 1975; *Pilipp et al.*, 1987a, 1987b] the relative densities of the nonthermal parts in the fast wind case are slightly higher compared to the slow wind one. The strahl relative density starts at 0.3 AU between 7 and 8% and falls to about 2% at 3 AU. The halo relative density, being less than 1% at the closest observed radial range to the Sun, reaches about 7% at 3 AU, i.e., about 4% more compared to the slow solar wind results.

[41] Regarding the non-Maxwellain character of eVDF tails in the fast wind, the radial evolution of the parameter κ for both the halo and the strahl components is qualitatively similar to the slow wind case. However, Figure 9 shows that at 0.3 AU the halo eVDF tails are already more non-Maxwellian than in the slow wind (compare Figure 5), while the relative densities are roughly the same.

[42] As for the slow wind case, we plot on Figure 10 the radial evolution of the model distribution function equation (1) for the fast wind. We compute the average values of all parameters at four radial bins: 0.35 AU (dotted line), 0.55 AU (dashed line), 0.75 AU (dash-dotted line) and 3 AU (solid line). Because of the lack of fast wind data samples, the furthest radial bin differs from Figure 6. The top left panel displays the overall model distribution, while in the other panels the model function and its

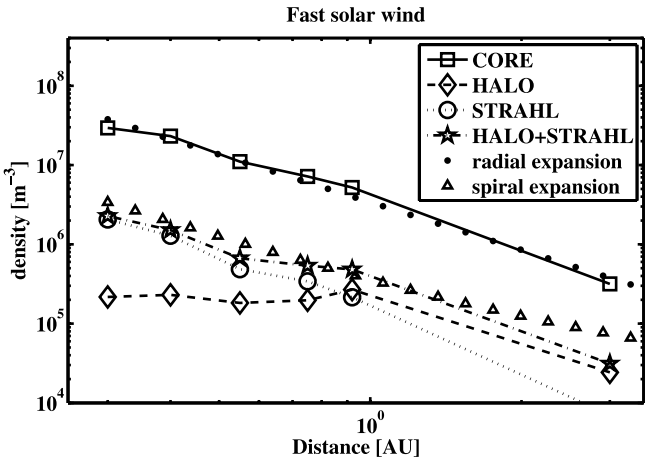

Figure 7. Radial evolution of the density profiles in the fast solar wind. As for the slow wind, the symbols represent the mean values as computed from the fitting results in several radial bins. The error bars are of the order of the symbol size. Theoretical reference profiles for an isotropic radial expansion and spiral expansion are plotted with dots and triangles, respectively. The solid line with squares, dashed line with diamonds, dotted line with circles, and dash-dotted line with stars represents the core, halo, strahl, and sum of strahl and halo, respectively.

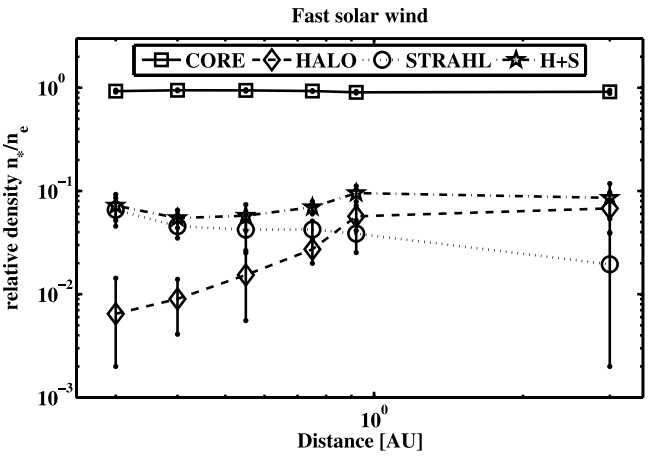

Figure 8. Fast wind radial evolution of the relative densities of the eVDF components. Symbols represent mean values and their error bars. The solid line with squares, dashed line with diamonds, dotted line with circles, and dash-dotted line with stars represents the core, halo, strahl, and sum of strahl a halo, respectively. The total number of nonthermal electrons remains almost constant along the observed range, strahl density is decreasing while halo grows at the same time. The sum of nonthermal components seems to be more variable than in the slow wind.

components are normalized with respect to the total density (y axis) and to the core thermal parallel velocity (x axis) again in order to remove the effects of the cooling and the rarefaction of the wind. The relative growth of the halo and the damping of the strahl as well as the decrease of the parameter κ for both of the nonthermal components are clearly visible on the bottom-left and bottom-right panel respectively. The basic trends in the radial evolution for the fast solar wind are actually very similar to those we have shown for the slow wind regime. However, the nominal values of the relative densities indicate on average stronger nonthermal tails.

4. Summary and Concluding Remarks

[43] We have proposed a new analytical model for the analysis of the measured eVDFs, which was shown to be convenient for fitting all three eVDF components typically observed in the solar wind, i.e., the core, the halo but also and for the first time the strahl. One of the main properties of the model is to fit the thermal and the nonthermal part of the observed eVDF separately. This our new model was applied on a large data set and the results were then examined separately for slow and fast solar wind observations. It is important to note that the all the conclusions concerning the fast wind case have to be taken with caution. Only about 10% of the total number of all eVDF samples represent the fast solar wind regime and the ratio is even smaller above 1 AU (i.e., Ulysses observations).

[44] Based on the fitting results, we have examined the relative densities of the three eVDF components and the importance of nonthermal eVDF tails as a function of the radial distance. We have shown that with increasing radial distance the strahl relative density decreases while the halo relative density increases, for both the slow fast solar wind regimes. For the slow wind, the total relative density of the nonthermal electrons, i.e., the sum of the halo and the strahl, remains almost constant in the whole observed radial range. The ratio of nonthermal electrons in the slow wind is found to be about 5–7%. In the fast wind the relative density of nonthermal electrons is more variable and grows

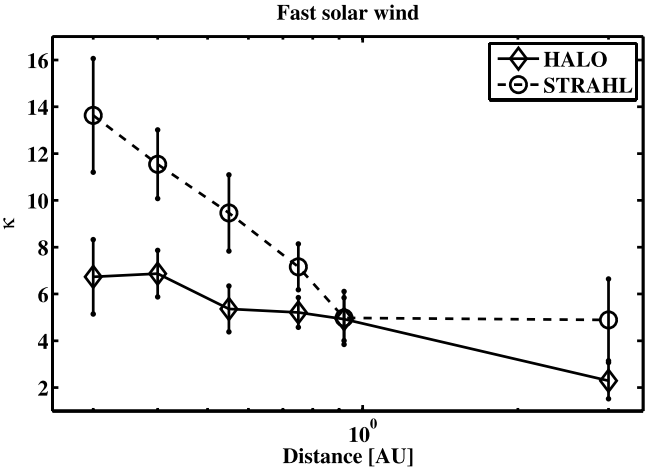

Figure 9. κ parameter can serve as a measure of the nonthermal state of an electron population. Here, we plot the mean κ parameter in the fast wind of the halo (dashed line with diamonds) and strahl component (dotted line with circles) as a function of the radial distance. Both of them are decreasing, indicating stronger eVDF tails at larger distances from the sun.

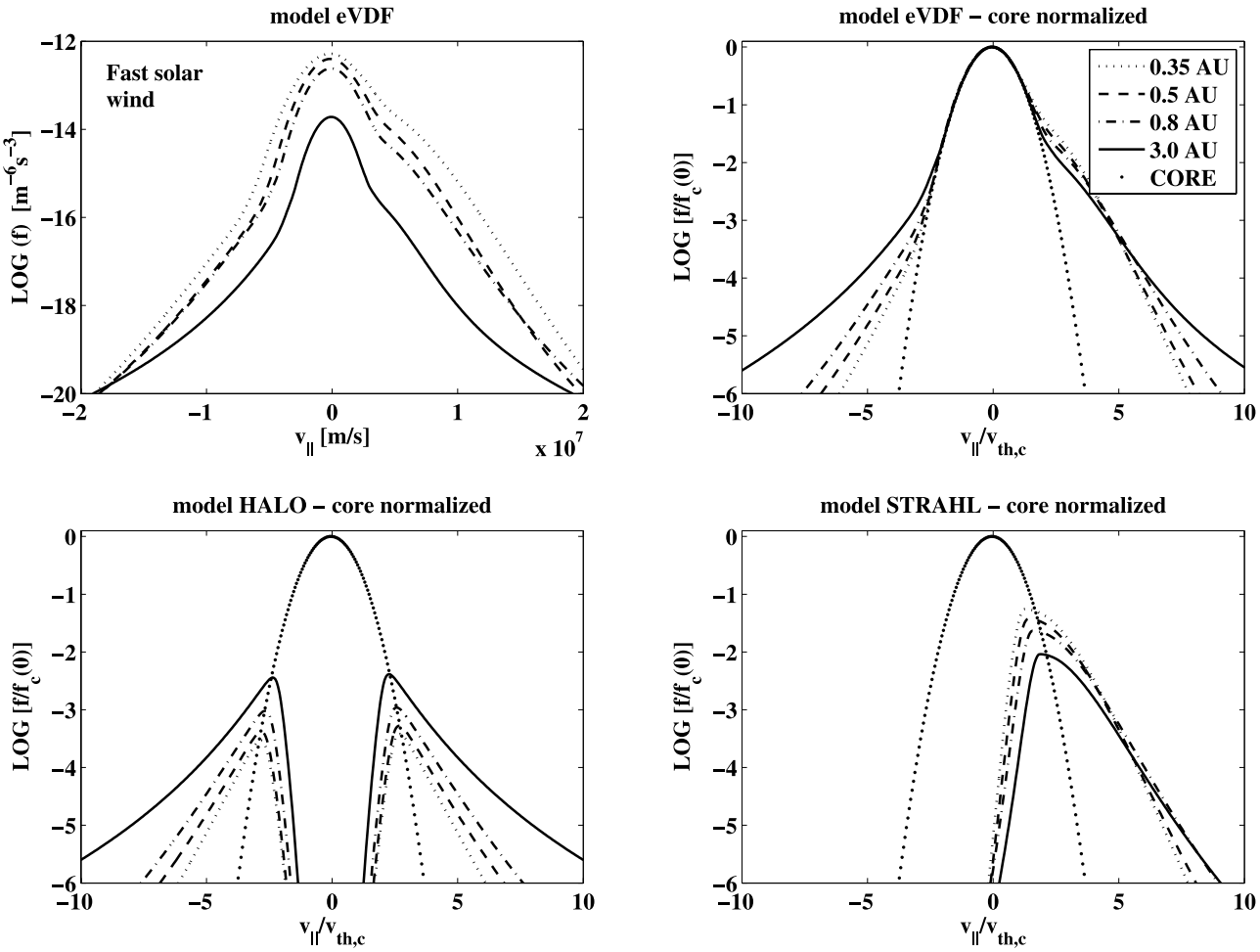

Figure 10. Radial evolution of a model eVDF function in the fast solar wind. Model functions are plotted using average values of all parameters resulting from the fitting at four different radial distances: 0.35 AU (dotted line), 0.55 AU (dashed line), 0.75 AU (dash-dotted line), and 3 AU (solid line). Except for the top left panel, the model eVDF functions are normalized in such a way that the value at the peak equals unity and the velocity is scaled by $v_{th,c}$. In the bottom panels, only the halo and strahl component evolution is compared with the normalized core. With increasing radial distance, the strahl electrons close to the thermal core are scattered while the halo develops stronger tails, slightly stronger than that in the slow wind.

up to about 10% close to 1 AU. The relative importance of nonthermal electrons in the fast solar wind seems to be slightly higher compared to the slow wind. This can be caused by typically lower densities observed in the fast wind, which makes the effect of Coulomb collisions less effective. The relatively stronger nonthermal eVDF tails in the fast wind can be, however, related to the slightly steeper gradient of the core density with respect to the slow wind case. Qualitatively, the relative densities presented in our study are similar to results found by *McComas et al.* [1992] and *Maksimovic et al.* [2005]. However, they are not fully comparable, since the model eVDFs used in the previous studies differ from the one used in the present work.

[45] As another characteristic of the nonthermal tails, we have examined the κ parameter of the model function used to fit the halo and strahl components. κ is decreasing with increasing radial distance from Sun for both the halo and the strahl. This indicates that the importance of nonthermal tails of eVDFs rises further from the Sun. In the slow wind the κ halo starts at 0.3 AU with a value of roughly 9.5 while in the fast wind the κ parameter is already less than 7. This shows that the fast wind has already more important nonthermal tails close to the Sun compared to the slow one [*Pilipp et al.*, 1987a, 1987b]. Smallest values, with a lower limit of 2, are observed at the largest radial distances. For the halo component in the fast wind, our results are again in fair agreement with *Maksimovic et al.* [2005] (see the bottom left panel on Figure 5 of the concerned paper).

[46] In order to summarize how the shape of observed eVDFs changes with increasing radial distance from Sun, we have also displayed the radial evolution of a mean model function, that is a model function computed from mean values of all its parameters. In general, our results are in agreement with those reported by *Maksimovic et al.* [2005] where only the fast solar wind was examined. Our results also support the scenario proposed by several authors [see

Gary et al., 1994; *Vocks et al.*, 2005; *Gary and Saito*, 2007; *Saito and Gary*, 2007] of strahl electrons being scattered into the halo. Adopting the scattering mechanisms, the observed radial evolution of nonthermal eVDF components likewise agrees with the numerical modeling of *Owens et al.* [2008] describing the expansion of nonthermal electrons on a background of spiral oriented magnetic field.

[47] As a byproduct of our fitting process, we have also analyzed the breakpoint energy, i.e., the limit energy where the nonthermal tails start to deviate from the Maxwellian core. Furthermore, we have examined the agreement between the relative core and strahl velocity drifts in the plasma frame and the zero-current condition. These results are shown and discussed in the appendices.

[48] In addition to the results provided in this paper, we can make a prediction concerning the eVDF properties outside the observed radial range. This prediction holds for both solar wind regimes, the slow one and the fast one. The more interesting edge of the interval, regarding the initial solar wind conditions, is the one pointing toward the Sun. Even though we cannot make any real conclusions about eVDFs in the coronal regions which are critical for the solar wind acceleration, our results seem to indicate that closer to the Sun, less than 0.3 AU, the fraction of halo electrons in high-energy tails tends to vanish. Vice versa, the strahl beam is possibly even stronger than what we observe beyond 0.3 AU. At the farther limit of the observed radial range, from our observations it is not clear whether or not the strahl will completely disappear, being after certain distance absorbed by the halo.

[49] There are many other aspects concerning the properties of the measured eVDFs in the solar wind, especially of the high-energy tails which we did not examine in this paper. For example, we did not study the angular distribution of the strahl electrons as it was done, for instance, by *Hammond et al.* [1996]. The majority of our data set comes from Helios measurements. In this case only eight angular bins are acquired which makes angular analysis less accurate. We have also presented most of the results only as a function of the heliocentric radial distance. In order to better understand the mechanisms responsible for the scattering of strahl electrons, we need to examine the evolution of the nonthermal eVDF tails with respect to the plasma collision properties and the observed activity of electromagnetic waves.

[50] Furthermore, in order to fully describe the properties and dynamics of the solar wind electrons, also other important moments of the eVDFs, such the temperature and the heat flux, have to be examined. In this paper we did not present the radial evolution of core temperatures, well defined by the bi-Maxwellian distribution. This subject was already examined and published by many other authors, we refer the reader, for example, to *Marsch et al.* [1989], *Issautier et al.* [1998], *Fludra et al.* [1999], or a summary in *Maksimovic et al.* [2000]. The situation is more complicated in the case of halo and strahl components where the distribution are completely different from Maxwellians. More interesting would be to study the relative dependence between the temperature or rather the effective kinetic pressure of the three eVDF components, as it was done in this study for their densities. We intend to present these results together with the heat flux properties, namely for the strahl component, in one of our next papers.

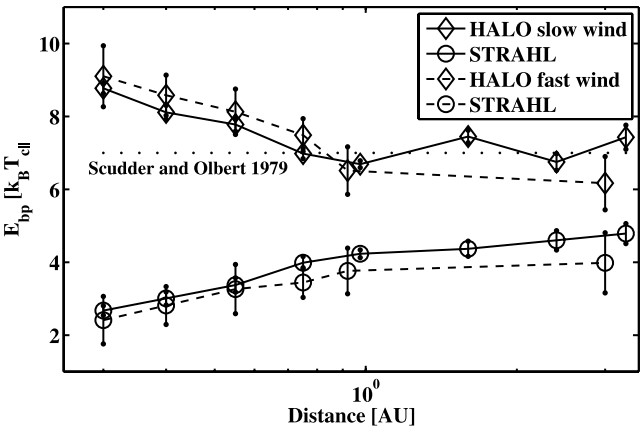

Figure A1. Radial evolution of the breakpoint energy E_{bp} normalized by $k_B T_{c\|}$. The halo breakpoint energy (dashed line with diamonds) is decreasing and reaching a theoretical limit (dots) around 0.8 AU. In this radial range, no upper limit is reached by the strahl breakpoint energy (dotted line with circles).

Appendix A: Breakpoint Energy

[51] Due to the properties of Coulomb collisions the solar wind electrons can be treated as a gas in a thermal equilibrium only up to certain energy level. Particles beyond this breakpoint energy E_{bp} have a minimal local interaction with surroundings and create nonthermal tails of the observed eVDFs. In the work of *Scudder and Olbert* [1979], the authors proposed that the observed eVDF in the solar wind are shaped primarily by Coulomb collisions. They conclude that the effect of Coulomb collisions by itself is sufficient to determine the shape of the eVDFs in both the thermal ($E < kT$) and suprathermal ($E > kT$) energy regimes. Furthermore, they theoretically predicted that the breakpoint energy scales with local temperature as

$$E_{bp}(r) \approx 7kT_C(r), \tag{A1}$$

where k is the Boltzmann constant and $T_C(r)$ is the local core electron temperature at the radial distance r.

[52] In this study we define two energy-normalized breakpoints, both in the parallel direction. One is defined in the sunward part of the eVDF: the halo energy breakpoint $E_{bp,h}$, and one in the antisunward direction: the strahl energy breakpoint $E_{bp,s}$. These normalized energies in units of $[kT_{c,\|}]$ are given as

$$E_{bp,*} = \frac{m v_{bp,*}^2}{2kT_{c\|}}, \tag{A2}$$

where the velocity $v_{bp,*}$ for halo and strahl is determined by

$$\begin{aligned} f_h(v_{bp,h}) &= f_c(v_{bp,h}) \\ f_s(v_{bp,s}) &= f_c(v_{bp,s}) + f_h(v_{bp,s}), \end{aligned} \tag{A3}$$

respectively. Results from our eVDF analysis are displayed on Figure A1. The dashed line with diamonds and the dotted line with circles represent the mean halo and strahl breakpoint energy, respectively, as a function of the heliocentric radial distance. The error bars of the mean values are expressed by vertical lines. The halo breakpoint energy slowly decreases with the increasing radial distance reaching the theoretical value of *Scudder and Olbert* [1979] between 0.7 and 0.8 AU. At larger distance it seems that this theoretical value represents a lower constraint, similar results are reported also by *McComas et al.* [1992]. An inverse trend is observed for the strahl breakpoint energy. The strahl breakpoint energy grows up with increasing radial distance and the slope of this growth is slowly decreasing. However, from this radial interval it is not clear whether the strahl breakpoint energy has some upper limit smaller than in the case of the halo. That is to say whether the strahl at a certain distance completely disappears or not. Actually, Figure A1 describes the radial evolution of competing halo and strahl components already demonstrated in the bottom panels of Figures 6 and 10.

Appendix B: Charge Flux

[53] In the solar wind, both ions and electrons are flowing together in the same direction. In order to maintain the global charge neutrality, no electric currents can exist in such an environment. This means that the ion and electron charge flux through a given area has to be equal. If the core and halo components would be flowing with the same velocity as the ions, the strahl electrons would break this equality and produce a nonzero current in the direction parallel with respect to the magnetic field. In order to satisfy the zero-current condition, i.e.,

$$v_{bulk,e} n_e = v_{bulk,ion} n_{ion}, \tag{B1}$$

in our model eVDF we allow not only the strahl drift Δ_s in equation (8) for $v_{\|}$ but also a drift of the core Δ_c in equation (2). For the model eVDF in the ion plasma frame the condition equation (B1) can be thus rewritten as

$$v_{bulk,c} n_c + v_{bulk,s} n_s = 0. \tag{B2}$$

During the fitting procedure we do not impose any dependence between Δ_c and Δ_s, both are completely independent. From the result we then compute the core charge flux Φ_c and strahl charge flux Φ_s as

$$\Phi_{c/s} = |v_{bulk,c/s}| n_{c/s}. \tag{B3}$$

According to equation (B2), both Φ_c and Φ_s have to be equal. These fluxes are compared on Figure B1. Here we plot the correlation between Φ_c and Φ_s separately for all three instruments used in our data set. We compute the mean values of Φ_s in several bins defined over the Φ_c range. Both slow and fast solar wind regimes are mixed on Figure B1 since the zero-current condition has to be valid in any case. For all three instruments, the fluxes are well correlated. However, except $\Phi_c \gtrsim 10^{12}\ e\ \mathrm{m}^{-2}\mathrm{s}^{-1}$ for Helios spacecraft, the fluxes do not exactly match the theoretical zero-current condition $\Phi_c = \Phi_s$. These discrepancies can result from many reasons. First, one should note that we use as a reference frame the proton bulk speed and that we neglect the alpha particles velocity. We are not therefore in the exact zero-current frame. Second, because of the large electron thermal speeds, the estimation of the drift velocities, namely for the core, can already contain a nonnegligible error. Also, the estimation of the density itself, especially for the strahl, can be inaccurate as well. Finally we have to take into account different designs of the instruments. For example, on Figure B1 we can see larger deviations from the mean values with decreasing charge flux which can be due to limited sensitivity of the individual sensors. All these facts put together make our fitting procedure acceptable corresponding to the zero-current condition and indicate that the strahl charge flux is balanced by the oppositely drifting core.

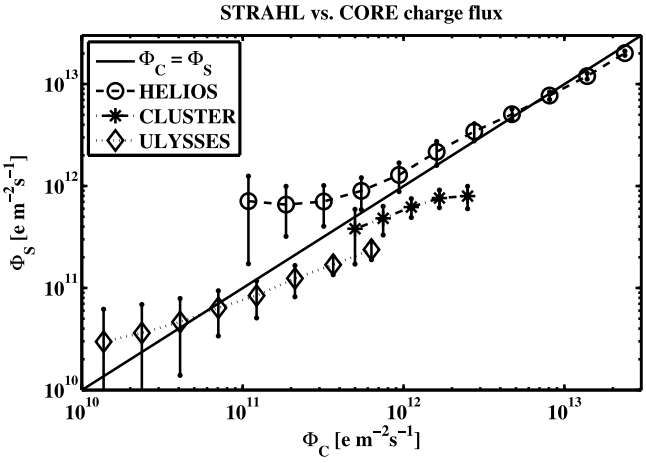

Figure B1. The charge flux of core Φ_c and strahl Φ_s is compared separately for all three spacecraft. We plot the mean values of Φ_s over all eVDF samples in several bins defined over the Φ_c range with circles, stars, and diamonds for Helios, Cluster, and Ulysses, respectively. The fluxes are well correlated for all three instruments. However, namely for Cluster and Ulysses, the correlation slightly deviates from the theoretical zero-current condition $\Phi_c = \Phi_s$. All analyzed data samples including observation of both slow and fast solar wind.

[54] Finally note that in our model we do not allow any drift for the halo component. If we suppose that the halo drifts together with the core, the halo contribution to the total electron charge flux will be negligible since the core drift is much smaller then the strahl drift while the densities of strahl and halo are comparable. Also, the estimate of the halo drift would be highly inaccurate because of the very large thermal speeds of halo electrons. Therefore an assumption of a nondrifting halo is acceptable. Furthermore, this assumption also makes the model and its analysis less complicated.

[55] **Acknowledgments.** The authors acknowledge the support of contracts IAA300420702 and IAA300420602 of Grant Agency of Academy of Sciences of the Czech Republic and contract PECS 98024 of European Space Agency.

[56] Amitava Bhattacharjee thanks Daniel Hubert and Mathew Owens for their assistance in evaluating this paper.

References

Bame, S. J., D. J. McComas, B. L. Barraclough, J. L. Phillips, K. J. Sofaly, J. C. Chavez, B. E. Goldstein, and R. K. Saturai (1992), The Ulysses

solar wind plasma experiment, *Astron. Astrophys. Suppl. Ser.*, *92*, 237–265.
Crooker, N. U., S. W. Kahler, D. E. Larson, and R. P. Lin (2004), Large-scale magnetic field inversions at sector boundaries, *J. Geophys. Res.*, *109*, A03108, doi:10.1029/2003JA010278.
Escoubet, C., R. Schmidt, and M. Goldstein (1997), Cluster: Science and mission overview, *Space Sci. Rev.*, *79*, 11–32.
Feldman, W., J. R. Asbridge, S. J. Bame, M. D. Montgomery, and S. P. Gary (1975), Solar wind electrons, *J. Geophys. Res.*, *80*, 4181–4196.
Fludra, A., G. Del Zanna, D. Alexander, and B. J. I. Bromage (1999), Electron density and temperature of the lower solar corona, *J. Geophys. Res.*, *104*, 9709–9720.
Gary, S. P., and S. Saito (2007), Broadening of solar wind strahl pitch-angles by the electron/electron instability: Particle-in-cell simulations, *Geophys. Res. Lett.*, *34*, L14111, doi:10.1029/2007GL030039.
Gary, S. P., E. E. Scime, J. L. Phillips, and W. C. Feldman (1994), The whistler heat flux instability: Threshold conditions in the solar wind, *J. Geophys. Res.*, *99*, 23,391–23,399.
Gosling, J. T., D. N. Baker, S. J. Bame, W. C. Feldman, R. D. Zwickl, and E. J. Smith (1987), Bidirectional solar wind electron heat flux events, *J. Geophys. Res.*, *92*, 8519–8535.
Gosling, J. T., S. J. Bame, W. C. Feldman, D. J. McComas, J. L. Phillips, and B. E. Goldstein (1993), Counterstreaming suprathermal electron events upstream of corotating shocks in the solar wind beyond ~2 AU: ULYSSES, *Geophys. Res. Lett.*, *20*, 2335–2338.
Gustafsson, G., et al. (1997), The electric field and wave experiment for the cluster mission, *Space Sci. Rev.*, *79*, 137–156, doi:10.1023/A:1004975108657.
Hammond, C. M., W. C. Feldman, D. J. McComas, J. L. Phillips, and R. J. Forsyth (1996), Variation of electron-strahl width in the high-speed solar wind: ULYSSES observations, *Astron. Astrophys.*, *316*, 350–354.
Hellinger, P., P. Trávníček, J. C. Kasper, and A. J. Lazarus (2006), Solar wind proton temperature anisotropy: Linear theory and WIND/SWE observations, *Geophys. Res. Lett.*, *33*, L09101, doi:10.1029/2006GL025925.
Issautier, K., N. Meyer-Vernet, M. Moncuquet, and S. Hoang (1998), Solar wind radial and latitudinal structure: Electron density and core temperature from ulysses thermal noise spectroscopy, *J. Geophys. Res.*, *103*, 1969–1979.
Johnstone, A. D., et al. (1997), Peace: A plasma electron and current experiment, *Space Sci. Rev.*, *79*, 351–398.
Kasper, J. C., A. J. Lazarus, S. P. Gary, and A. Szabo (2003), Solar wind temperature anisotropies, in *Solar Wind Ten, American Institute of Physics Conference Series*, vol. 679, edited by M. Velli et al., pp. 538–541.
Lamy, H., V. Pierrard, M. Maksimovic, and J. F. Lemaire (2003), A kinetic exospheric model of the solar wind with a nonmonotonic potential energy for the protons, *J. Geophys. Res.*, *108*(A1), 1047, doi:10.1029/2002JA009487.
Lemaire, J., and M. Scherer (1971), Kinetic models of the solar wind, *J. Geophys. Res.*, *76*, 7479–7490.
Lie-Svendsen, Ø., V. H. Hansteen, and E. Leer (1997), Kinetic electrons in high-speed solar wind streams: Formation of high-energy tails, *J. Geophys. Res.*, *102*, 4701–4718.
Maksimovic, M., V. Pierrard, and J. F. Lemaire (1997a), A kinetic model of the solar wind with Kappa distribution functions in the corona, *Astron. Astrophys.*, *324*, 725–734.
Maksimovic, M., V. Pierrard, and P. Riley (1997b), Ulysses electron distributions fitted with Kappa functions, *Geophys. Res. Lett.*, *24*, 1151–1154.
Maksimovic, M., S. P. Gary, and R. M. Skoug (2000), Solar wind electron suprathermal strength and temperature gradients: Ulysses observations, *J. Geophys. Res.*, *105*, 18,337–18,350.
Maksimovic, M., V. Pierrard, and J. Lemaire (2001), On the exospheric approach for the solar wind acceleration, *Astrophys. Space Sci.*, *277*, 181–187, doi:10.1023/A:1012250027289.
Maksimovic, M., et al. (2005), Radial evolution of the electron distribution functions in the fast solar wind between 0.3 and 1.5 au, *J. Geophys. Res.*, *110*, A09104, doi:10.1029/2005JA011119.
Marquardt, D. (1963), An algorithm of least-squares estimation of nonlinear parameters, *J. Appl. Math.*, *11*, 431–441.
Marsch, E. (2006), Kinetic physics of the solar corona and solar wind, *Living Rev. Sol.*, *3*, 1–100.
Marsch, E., K. M. Thieme, H. Rosenbauer, and W. G. Pilipp (1989), Cooling of solar wind electrons inside 0.3 AU, *J. Geophys. Res.*, *94*, 6893–6898.
Marsch, E., L. Zhao, and C.-Y. Tu (2006), Limits on the core temperature anisotropy of solar wind protons, *Ann. Geophys.*, *24*, 2057–2063.
McComas, D. J., S. J. Bame, W. C. Feldman, J. T. Gosling, and J. L. Phillips (1992), Solar wind halo electrons from 1–4 AU, *Geophys. Res. Lett.*, *19*, 1291–1294.
Montgomery, M. D., S. J. Bame, and A. J. Hundhausen (1968), Solar wind electrons: Vela 4 measurements, *J. Geophys. Res.*, *73*, 4999–5003.
Owens, M. J., N. U. Crooker, and N. A. Schwadron (2008), Suprathermal electron evolution in a Parker spiral magnetic field, *J. Geophys. Res.*, *113*, A11104, doi:10.1029/2008JA013294.
Parker, E. N. (1963), *Interplanetary Dynamical Processes*, Wiley-Interscience, Hoboken, N. J.
Pierrard, V., and J. Lemaire (1996), Lorentzian ion exosphere model, *J. Geophys. Res.*, *101*, 7923–7934.
Pierrard, V., M. Maksimovic, and J. Lemaire (1999), Electron velocity distribution functions from the solar wind to the corona, *J. Geophys. Res.*, *104*, 17,021–17,032.
Pierrard, V., M. Maksimovic, and J. Lemaire (2001), Self-consistent model of solar wind electrons, *J. Geophys. Res.*, *106*, 29,305–29,312.
Pilipp, W. G., K.-H. Muehlhaeuser, H. Miggenrieder, M. D. Montgomery, and H. Rosenbauer (1987a), Characteristics of electron velocity distribution functions in the solar wind derived from the HELIOS plasma experiment, *J. Geophys. Res.*, *92*, 1075–1092.
Pilipp, W. G., K.-H. Muehlhaeuser, H. Miggenrieder, H. Rosenbauer, and R. Schwenn (1987b), Variations of electron distribution functions in the solar wind, *J. Geophys. Res.*, *92*, 1103–1118.
Rosenbauer, H., et al. (1977), A survey on initial results of the HELIOS plasma experiment, *J. Geophys. Zeitschr. für Geophys.*, *42*, 561–580.
Saito, S., and S. P. Gary (2007), Whistler scattering of suprathermal electrons in the solar wind: Particle-in-cell simulations, *J. Geophys. Res.*, *112*, A06116, doi:10.1029/2006JA012216.
Salem, C., J.-M. Bosqued, D. E. Larson, A. Mangeney, M. Maksimovic, C. Perche, R. P. Lin, and J.-L. Bougeret (2001), Determination of accurate solar wind electron parameters using particle detectors and radio wave receivers, *J. Geophys. Res.*, *106*, 21,701–21,717.
Schwenn, R., H. Rosenbauer, and H. Miggenrieder (1975), Das Plasmaexperiment auf Helios, *Raumfahrtforschung*, *19*, 226.
Scime, E. E., S. J. Bame, W. C. Feldman, S. P. Gary, J. L. Phillips, and A. Balogh (1994a), Regulation of the solar wind electron heat flux from 1 to 5 AU: ULYSSES observations, *J. Geophys. Res.*, *99*, 23,401–23,410.
Scime, E. E., J. L. Phillips, and S. J. Bame (1994b), Effects of spacecraft potential on three-dimensional electron measurements in the solar wind, *J. Geophys. Res.*, *99*, 14,769–14,776.
Scudder, J. D. (1992), Why all stars should possess circumstellar temperature inversions, *Astrophys. J.*, *398*, 319–349, doi:10.1086/171859.
Scudder, J. D., and S. Olbert (1979), A theory of local and global processes which affect solar wind electrons: I. The origin of typical 1 AU velocity distribution functions - steady state theory, *J. Geophys. Res.*, *84*, 2755–2772.
Song, P., X. X. Zhang, and G. Paschmann (1997), Uncertainties in plasma measurements: Effect of lower cutoff energy and spacecraft charge, *Planet. Space Sci.*, *45*, 255–267.
Štverák, Š., P. Trávníček, M. Maksimovic, E. Marsch, A. N. Fazakerley, and E. E. Scime (2008), Electron temperature anisotropy constraints in the solar wind, *J. Geophys. Res.*, *113*, A03103, doi:10.1029/2007JA012733.
Vocks, C., C. Salem, R. P. Lin, and G. Mann (2005), Electron halo and strahl formation in the solar wind by resonant interaction with whistler waves, *Astrophys. J.*, *627*, 540–549, doi:10.1086/430119.
Zouganelis, I., M. Maksimovic, N. Meyer-Vernet, H. Lamy, and K. Issautier (2004), A transonic collisionless model of the solar wind, *Astrophys. J.*, *606*, 542–554, doi:10.1086/382866.

A. N. Fazakerley, Mullard Space Science Laboratory, University College of London, Holmbury St. Mary, RH5 6NT Dorking, UK.
M. Maksimovic, LESIA, Observatoire de Paris, CNRS, UPMC, Université Paris Diderot, bat. 16, 5 pl. J. Janssen, 92195 Meudon, France.
E. Marsch, Department for Sun and Heliosphere, Max Planck Institute for Solar System Research, Max-Planck-Strasse 2, D-37191 Katlenburg-Lindau, Germany.
E. E. Scime, Department of Physics, West Virginia University, Box 6315, Morgantown, WV 26506, USA.
Š. Štverák, Department of Space Physics, Institute of Atmospheric Physics, Academy of Sciences of the Czech Republic, Bocni II 1401, Prague 141 31, Czech Republic. (stverak@ufa.cas.cz)
P. M. Trávníček, Solar Physics Department, Astronomical Institute, Academy of Sciences of the Czech Republic, Bocni II 1401, Prague 141 31, Czech Republic.